Environmental Science and Pollution Research (2023) 30:123055–123066
https://doi.org/10.1007/s11356-023-30960-4

RESEARCH ARTICLE

Performance evaluation of sulfidated nanoscale iron for hexavalent chromium removal from groundwater in sequential batch study

Mainak Bhattacharya[1] · **Najmul Haque Barbhuiya**[1] · **Swatantra P. Singh**[1,2,3,4]

Received: 16 July 2023 / Accepted: 4 November 2023 / Published online: 18 November 2023

Abstract

Chromium [Cr] contamination in groundwater is one of the serious environmental concerns due to the carcinogenicity of its water-soluble and mobile hexavalent [Cr(VI)] form. In spite of the existence of multiple precipitation and adsorption-based Cr(VI) remediation technologies, the usage of sulfidated nano zerovalent iron (S-nZVI) has recently attracted researchers due to its high selectivity. Although S-nZVI effectively immobilized Cr(VI), its long-term performance in multiple shifted equilibrium has not been explored. In this contribution, influences of S-nZVI dosage, initial concentration of Cr(VI), pH, ionic strength, total hardness, sulfate, carbonate, and silicate were probed in ultrapure water. Further experiments were performed in synthetic groundwater to investigate the effects of initial concentration of Cr(VI) in the pH range of 4–8 for 1 g L^{-1} S-nZVI dosage. Cr(VI) removal rate was quantified in groundwater without pH fixation. Finally, a comparative study between conventional nano zerovalent iron (nZVI) and S-nZVI was conducted in sequential batch reactors to investigate their respective efficiencies during repeated usage. Mechanistic interpretation of the processes governing the immobilization of Cr(VI) was done by integrating the results of these experiments with the metadata. While aggregation due to magnetic properties and rapid oxidation of Fe decreased the efficiency of nZVI with repeated usage, sulfidation minimized the passivation and favored an extended reducing environment because of continuous electron transfer from iron and sulfur components.

Keywords Sulfidized nano zerovalent iron · Chromium · Groundwater · Reactive life · Longevity · Kinetic modeling

Responsible Editor: Ioannis A. Katsoyiannis

Highlights

- Enhanced Cr(VI) removal was observed in the presence of high dissolved SO_4^{2-}.
- Increased ionic strength of the background matrix aided in higher Cr(VI) removal.
- Cr(VI) reduction by S-nZVI followed second-order reaction kinetics.
- S-nZVI showed better long-term performance than nZVI in sequential groundwater batches.

✉ Swatantra P. Singh
swatantra@iitb.ac.in

[1] Environmental Science and Engineering Department, Indian Institute of Technology Bombay, Mumbai 400076, India

[2] Interdisciplinary Program in Climate Studies, Indian Institute of Technology Bombay, Mumbai 400076, India

[3] Centre for Research in Nanotechnology & Science, Indian Institute of Technology Bombay, Mumbai 400076, India

[4] Centre of Excellence On Membrane Technologies for Desalination, Brine Management, and Water Recycling (DeSaltM), Indian Institute of Technology Bombay, Mumbai 400076, India

Introduction

The presence of chromium [Cr] in groundwater aquifers is a global environmental concern (Bacquart et al. 2015; Santra et al. 2018; Kanagaraj and Elango 2019; Poonia et al. 2021). The drinking water standards for Cr recommended by the US Environmental Protection Agency (USEPA) is 0.1 mg L^{-1} (USEPA 2022). While hexavalent chromium [Cr(VI)] is highly soluble, mobile, and carcinogenic, its reducing counterpart trivalent chromium [Cr(III)] is insoluble, less mobile, and non-toxic (Rai et al. 1987; Sass and Rai 1987; Turick et al. 1996). One of the common pathways of immobilization of soluble Cr in groundwater is to add a reducing agent, such as iron sulfate or nanoscale zerovalent iron (nZVI), to cause a reduction of soluble Cr(VI), resulting in the precipitation of insoluble Cr(III) (Qin et al. 2005; Sharma et al. 2008; Gheju 2011). However, nZVI might also remove non-target hydrophilic contaminants, decreasing the extent of Cr(VI) reduction and thereby increasing the treatment cost (Guan et al. 2015; Dai et al. 2022).

Recently, sulfidized nanoscale zerovalent iron (S-nZVI) has been identified as one of the most suitable materials due to its potential benefits in groundwater treatment (Shen et al. 2021; Xu et al. 2021b). Sulfidation of zerovalent iron (ZVI) increased specific surface area and improved ZVI's reactivity, selectivity, longevity, and electron utilization (Fan et al. 2017; Xu et al. 2019). Moreover, sulfur induction increases hydrophobicity, blocks hydrogen adsorption, and redistributes charge density (Xu et al. 2021b). All these properties of S-nZVI benefit the remediation of typical groundwater contaminants. Chen et al. (2022) showed improvement in the performance of nZVI when it was modified with sulfur and proposed that sulfur-modified nZVI has the potential to solve the issue of dissolved heavy metal contamination in environmental matrices (Wei et al. 2021; Chen et al. 2022).

In the last few years, several researchers successfully demonstrated the removal of dissolved Cr(VI) by S-nZVI in Cr(VI)-spiked synthetic water matrices (Lv et al. 2019; Brumovský et al. 2021; Dai et al. 2022). In S-nZVI, Fe and S coatings contain phases like $FeS_{(s)}$ or $FeS_{2(s)}$, along with Fe^0. This results in the inhibition of particle agglomeration, increase in specific surface area, and improvement in remediation efficiency of Cr(VI). The mechanism of Cr(VI) removal by S-nZVI includes adsorption of Cr(VI) and reduction of Cr(VI) to insoluble and immobile Cr(III) (Gong et al. 2017). Lv et al. (2019) also proposed the removal of Cr(VI) by S-nZVI as a multi-step process involving instantaneous reduction of Cr(VI), followed by coprecipitation and adsorption (Lv et al. 2019). The processes governing Cr(VI) immobilization might vary in different kinds of modified S-nZVI. For example, most of the dissolved Cr(VI) was adsorbed on zeolite-supported S-nZVI (Zhou et al. 2022), but an integrated adsorption and reduction process was responsible for the removal of Cr(VI) by oyster shell powder supported S-nZVI (Hu et al. 2022). Past researchers further suggested that initial ultrasonication for an optimum period of 10 min exhibited improved sulfidation, resulting in enhanced Cr(VI) remediation (Dai et al. 2022). Moreover, high temperature, rising ionic strength, and low pH were found to be the dominating parameters responsible for high treatment efficiency (Lv et al. 2019). Removal of Cr(VI) by S-nZVI was reported to be an acid-driven surface-mediated process with maximum efficiency at pH 2.5 (Gao et al. 2018). It was further reported that dissolved sulfate led to higher removal of Cr(VI), but the efficiency varied inversely proportionately to the dissolved calcium level (Gao et al. 2018). Another study with blast furnace slag-supported modified S-nZVI stated that dissolved nitrate and humic acid affected Cr(VI) remediation from aqueous solution (Deng et al. 2020). In spite of some of the aforementioned limitations, S-nZVI proved to be more effective in the remediation of dissolved Cr(VI) than other toxic heavy metals like lead, nickel, and cadmium (Wei et al. 2021). It was reported that in a mixed metal matrix, biochar supported modified S-nZVI could increase the removal efficiency of Cr(VI) by 9.2% and decrease the removal of cadmium by 43.47% (Zhao et al. 2022).

Researchers have also compared the performance of S-nZVI with different types of modified S-nZVI. For example, Xi et al. (2022) established that comparatively higher Cr(VI) was recovered when S-nZVI was covered with an extracellular polymeric substance (Xi et al. 2022). Humic acid and unmodified FeS can remove Cr(VI), but humic acid stabilized FeS showed enhanced Cr(VI) remediation even in the presence of high Cr(VI) (Yao et al. 2020). Polysulfide-modified nZVI reportedly contributed to Cr(VI) removal from groundwater (Yu et al. 2023). However, the performance of the modified S-nZVI during its repetitive usage in the treatment of sequential batches of Cr(VI) contaminated water is not well established. Furthermore, the S-nZVI performance in groundwater matrix and the possibility of an extended reactive lifetime in aqueous solution have not been explored. This contribution attempted to treat multiple batches of highly contaminated groundwater matrix with S-nZVI and nZVI particles to compare their respective performances. Recovering and reusing the nanoparticles in sequential batches in the laboratory scale would provide insight into the possibility of their application for low-cost treatment. The specific objectives of the present research are (a) to demonstrate the removal of Cr(VI) from ultrapure water and groundwater matrices under varying geochemical conditions, (b) to estimate the rate of Cr(VI) removal by S-nZVI in groundwater, and (c) to compare the long-term performance of nZVI and S-nZVI in sequential batches of Cr(VI) contaminated water.

Materials and methods

Synthesis of S-nZVI

Synthesis of S-nZVI was carried out by the borohydride reduction method (Xu et al. 2020a; Cao et al. 2021). A solution of 10 g L^{-1} of trivalent iron was prepared by adding ferric chloride [$FeCl_3$] in 100 mL ultrapure water and purged continuously with nitrogen. Another 100 mL solution containing 2.2 g L^{-1} sodium dithionite ($Na_2S_2O_4$) and 34 g L^{-1} sodium borohydride ($NaBH_4$) was separately prepared and dropwise added to the Fe(III) solution with continuous nitrogen purging. This one-step method of S-nZVI synthesis with the addition of $Na_2S_2O_4$ was followed in the present study because it was reported to provide better longevity and reactivity (Xu et al. 2019). After the complete mixing of the two solutions, nitrogen purging was stopped. The formation of black-colored particles was visually observed. These particles were carefully transferred in 50 mL centrifuge tubes and washed once with ultrapure water and thrice with ethanol.

Cleaned particles were centrifuged at 2500 rpm for 15 min. The supernatant was decanted, and the solid residues were gently blown with nitrogen before vacuum drying for 3 h at 80 °C. The dried particles were stored in capped centrifuge tubes inside a desiccator at 25 °C for characterization and experiments. Similar protocols, except the step of addition of $Na_2S_2O_4$, were followed to synthesize nZVI and described in the Supporting Information (SI, Section S1).

Batch equilibration experiments

Batch reactors were set up to demonstrate the influence of various parameters responsible for the remediation of dissolved Cr(VI) by S-nZVI in an ultrapure water matrix. For all the experiments, Cr(VI) was spiked in these reactors as $K_2Cr_2O_7$. Initially, the effect of the dosage of S-nZVI was studied in batch reactors contaminated with 20 mg L^{-1} Cr(VI). The mass concentration of S-nZVI was varied from 0.25 to 2 g L^{-1}. S-nZVI dosage of 1 g L^{-1} was used as a constant solid concentration for all the experiments performed afterward. Effects of the initial concentration of Cr(VI) were studied in the range of 2–100 mg L^{-1}. Consequently, influences of other physicochemical parameters such as ionic strength, divalent cations naturally present in groundwater contributing to its hardness (calcium, magnesium), divalent anions that might compete with chromate (sulfate, silicate, carbonate), and pH were studied at 20 mg L^{-1} initial Cr(VI). The effect of ionic strength was probed in NaCl solution at a concentration range of 1–100 mM. Since hardness in drinking water is governed by its calcium (Ca) and (Mg) content, $CaCl_2$ and $MgCl_2$ salts were added in ultrapure water at varying quantities to determine the effect of total hardness. Effects of sulfate, silicate, and carbonate were studied by adding respective amounts of Na_2SO_4, Na_2SiO_3, and Na_2CO_3 in the water matrix. The influence of solution pH was investigated between pH 4 and 8.5. Solutions of 0.01 M HNO_3 and 0.01 M NaOH were used for pH adjustment.

Remediation of Cr(VI) by S-nZVI was further investigated in a synthetic groundwater matrix containing typical background analytes (Matern et al. 2017; Bhattacharya et al. 2020) of contaminated aquifers in India (Section S2, Table S1). Synthetic groundwater was prepared by dissolving $CaCl_2{\cdot}2H_2O$ (147 mg), $MgSO_4{\cdot}7H_2O$ (246 mg), NaCl (176 mg), KNO_3 (16 mg), $NaHCO_3$ (14 mg), and dextrose (10 mg) in ultrapure water (1 L) to meet the respective concentration ranges of the solutes (Matern et al. 2017; Bhattacharya et al. 2020). Cr(VI) concentration in these reactors was varied from 2 to 100 mg L^{-1} in the pH range of 4–8. A consistent S-nZVI dosage of 1 g L^{-1} was maintained in the batch reactors. The reactors were loaded on a horizontal shaker and mixed at 120 rpm. All the equilibration experiments were performed for a duration of 24 h.

Kinetic study

The kinetics of Cr(VI) removal was investigated in the synthetic groundwater matrix for an initial Cr(VI) concentration of 20 mg L^{-1} in sacrificial batch reactors. A constant S-nVZI dosage of 1 g L^{-1} was applied and loaded on a horizontal shaker for mixing at 120 rpm. Liquid samples were collected with time for Cr(VI) and pH measurements. Dedicated batch reactors were set up for each time point, which was sacrificed immediately after the collection of samples. The kinetic data were modeled to determine the rate of Cr(VI) remediation. The data were fitted in conventional first-order (Eq. 1) and second-order (Eq. 2) reaction models. These equations are derived by assuming that the rate of change in pollutant concentration ($-dC/dt$) is directly proportional to the nth power of the concentration of the pollutant at any time t for nth order reaction (C^n). A constant rate value (k) was assumed, and multiple iterations were done by changing this value through minimum mean square error. In this mathematical exercise, the sum of the squares of the differences between the modeled Cr(VI) and experimentally determined Cr(VI) was minimized by varying the rate constant. Correlation coefficients of the modeled data for first- and second-order reactions were compared.

$$CrVI_t = CrVI_0 e^{-kt} \tag{1}$$

$$CrVI_t = \frac{1}{(kt) + \frac{1}{CrVI_0}} \tag{2}$$

In Eqs. 1 and 2, time and reaction rate constant have been denoted as t and k, respectively. The unit of t is minute. For the first-order reaction (Eq. 1), the unit of k is min^{-1}. In the second-order reaction (Eq. 2), k is represented in L mg^{-1} min^{-1}. Respective concentrations of Cr(VI) at time zero and any time t have been represented by $CrVI_0$ and $CrVI_t$ in mg L^{-1}.

Sequential batch extraction experiments

The feasibility of repeated usage of S-nZVI was investigated in 20 mg L^{-1} Cr(VI) spiked ultrapure and synthetic groundwater matrices. S-nZVI, at mass concentration 1 g L^{-1}, was added in Cr(VI)-spiked batch reactors and loaded on a horizontal shaker for mixing at 120 rpm. Liquid samples were collected after 24 h for Cr(VI) measurement. The rest of the solution was carefully decanted after centrifugation at 4000 rpm for 15 min. Prevention of loss of the leftover solid residues was ensured by inserting a magnet while decanting. The recovered solids were reacted with another batch of 20 mg L^{-1} Cr(VI) solution. This process of the sequential

batch experiment was repeated for five cycles. After the final cycle, the recovered solids were centrifuged and oven-dried at 40 °C for X-ray diffraction (XRD) analysis. One of the replicates was sacrificed after the first cycle of the batch for XRD analysis of the leftover solid. Measurements of Cr(VI) and pH were done at the end of each cycle. Similar experiments in parallel were also performed with conventional nZVI following identical protocols to compare the efficiency of S-nZVI with nZVI during repetitive usage.

Analytical methods

Liquid phase characterization included measurements of pH, Cr(VI), total Cr, and Fe. Solution pH was measured using a glass electrode and benchtop meter (AZ Company 86502). Liquid samples were filtered through 0.2 µm syringe filters, and Cr(VI) was measured using the spectrophotometric technique in an ultraviolet–visible spectrophotometer (Thermo Scientific), following the di-phenyl carbazide method (USEPA 1992). In this method, 10 mL of filtered liquid samples were added with three drops of concentrated orthophosphoric acid and 0.2 mL di-phenyl carbazide (DPC) solution. The DPC solution was prepared by dissolving 250 mg DPC salt in 50 mL acetone and preserved in a brown bottle wrapped up with aluminum foil to minimize the influence of sunlight. Approximately 10–12 min of time was given for color development after the addition of orthophosphoric acid and DPC in the filtered liquid samples. Thereafter, the absorbance of the liquid samples was recorded at 540 nm wavelength in UV–Vis. The instrument was calibrated in the Cr(VI) concentration range of 0.05–2 mg L^{-1}, prior to analysis of the samples. Whenever required, the samples were diluted to bring the Cr(VI) level within the calibration range, and multiplied by the dilution factor to estimate the actual Cr(VI) concentration after noting down the absorbance. Total Cr and Fe were measured using the inductively coupled plasma atomic emission spectroscopy (ICP-AES) (SPECTRO Analytical Instruments). For ICP-AES analysis, an aliquot of each of the filtered samples was acidified using concentrated HNO_3. The acidification was done maintaining 1% acid fraction on volume-to-volume basis in the filtered liquid aliquot. There was no requirement of dilution as ICP-AES was calibrated in the broad range of 0.05–100 mg L^{-1}, prior to analysis of the acidified samples. The chemicals used for this study were of analytical grade or better purity. All the mathematical modeling was performed using the Solver and Data Analysis Tool Pack of Microsoft Excel 2016.

Solid phase characterization was performed on S-nZVI particles to determine the mineralogy, morphology, and elemental profiles. The mineralogical composition of S-nZVI was determined by XRD (PANalytical, X'Pert Pro) technique. The diffraction pattern was recorded in the range of 10 to 100° 2θ, and the data was processed through the MDI JADE (International Centre for Diffraction Data 2010) software. Scanning electron microscopy (SEM) and associated energy-dispersive X-ray (EDX) (JEOL JSM-7600F) analyses were performed to obtain the morphology and elemental profile of S-nZVI, respectively, at an accelerating voltage range of 0.1 to 10 keV. The nanostructure of S-nZVI solid was captured using high-resolution transmission electron microscopy (TEM) (Thermo Scientific, Themis 300 G3) technology at 300 kV. EDX area mapping was further done on these TEM images captured at the nanoscale to find the elemental composition of S-nZVI at a reducing interaction volume. The oxidation states of Cr in the solid residues after the reaction were determined by X-ray photoelectron spectroscopy (XPS) (ULVAC-PHIPHI5000, Versa Probe II). All the instruments were properly calibrated prior to usage. The point of zero charge (pZC) of the synthesized S-nZVI was estimated by the method of salt addition (SI, Section S3) following the methodology suggested by a previous study (Mahmood et al. 2011).

Results and discussion

Characterization of S-nZVI

XRD analysis of S-nZVI confirmed the presence of both iron [Fe] and iron-sulfur [FeS_2] phases in the synthesized solid (Fig. 1a). The mineralogical composition of S-nZVI depends on the chemicals used for sulfurization. Usage of $S_2O_4^{2-}$ as the precursor resulted in the formation of the FeS_2 phase, and this observation is consistent with previous research where the crystalline structure of S-nZVI affected by various S-bearing compounds, utilized to synthesize S-nZVI, was probed (Xu et al. 2020a). The powder diffraction file (PDF), 98–000-0259, matched with the most intense peak of the diffraction pattern (ICDD 2013) at 2θ of 44.67°. This peak corresponds to Fe^0 for the lattice plane of 110 (hkl). The diffraction pattern of S-nZVI matched with one more peak of the aforementioned PDF at 2θ value 82.33° for the miller index of 220 (hkl). The FeS_2 peak in the form of marcasite was found in the synthesized S-nZVI solid at 2θ 33.5°. This peak matched with the most intense peak of the diffraction pattern of PDF 01–074-1051 for FeS_2 lattice plane 020 (hkl). Since pyrite-like mineralogical phases [FeS_2] are more hydrophobic than mackinawite-like solids [FeS] (Gu et al. 2019; Xu et al. 2020a, b), the S-nZVI synthesized for this study is expected to aid in contaminant removal due to high hydrophobicity. SEM–EDX analysis of S-nZVI indicated the presence of spherical-shaped particles (Fig. 1b) containing Fe and S. Approximate estimation of atomic percentage of Fe and S was obtained from SEM-associated EDX analysis. For a better interpretation of the morphology, TEM analysis was done at nanometer scale, demonstrating

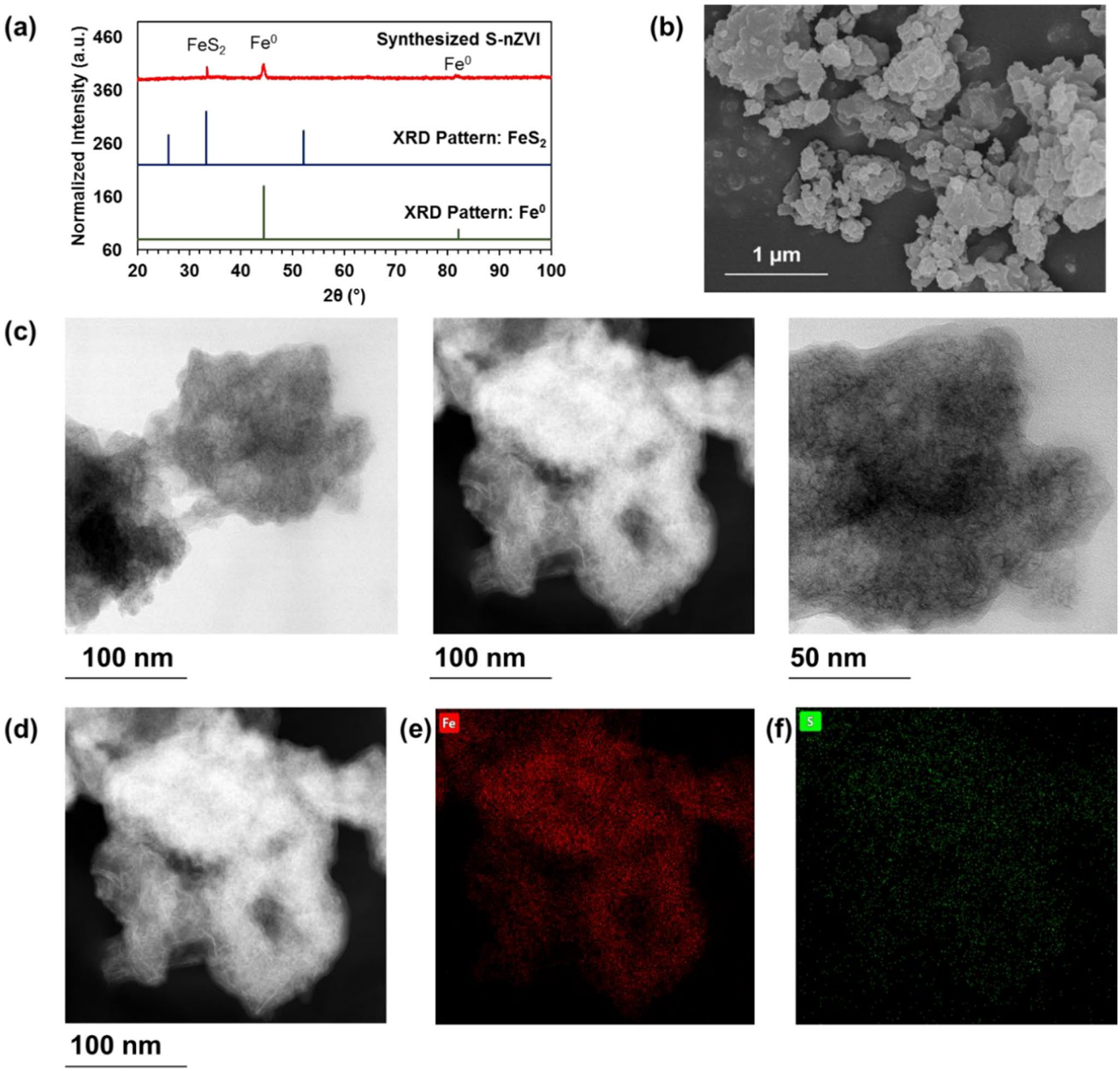

Fig. 1 **a** XRD analysis, **b** SEM imaging, **c** TEM imaging at two different magnifications, and **d** TEM imaging at 100 nm magnification with associated EDX area mapping for **e** Fe and **f** S of the synthesized S-nZVI. Identified peaks of the XRD pattern of the solid have been labeled as FeS_2 for PDF 01–074-1051, and Fe^0 for PDF 98–000-0259. The respective atomic percentage of Fe and S determined by SEM-associated EDX analysis was 20.88% and 1.03%. Identification of Fe and S through area mapping of the TEM image have been denoted in red and green colors, respectively

nanocrystals and nanosheet structures of S-nZVI particles (Fig. 1c). These kinds of structures were previously reported to cause lesser agglomeration as compared to conventional nZVI (Chen et al. 2022). EDX area mapping associated with high-resolution TEM (Fig. 1d) justified these findings as dispersion of both Fe and S was observed throughout the particle (Fig. 1 e and f). The area mapping analysis confirmed the successful modification of iron nanoparticles with S. XRD analysis of nZVI indicated the presence of only Fe^0, which has been demonstrated later in Sect. 3.4.

Physicochemical parameters affecting Cr(VI) removal

The addition of S-nZVI in water resulted in rise in equilibrium pH (Fig. 2a). Cr(VI) concentration decreased with the

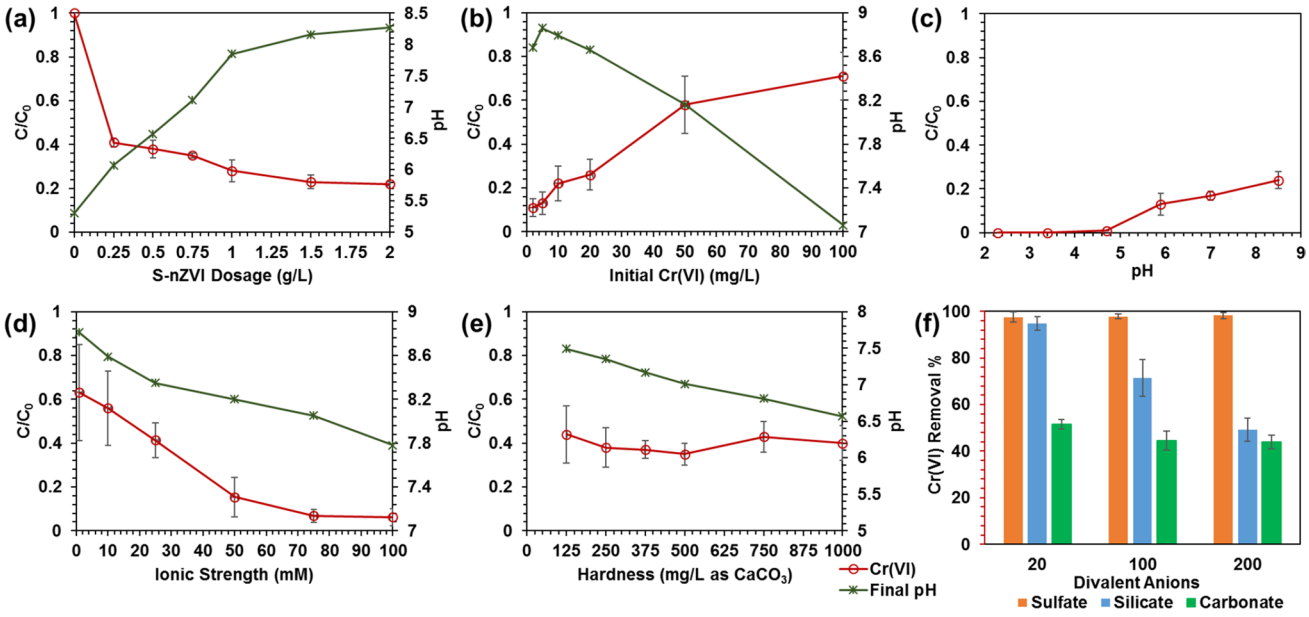

Fig. 2 Influence of **a** S-nZVI dosage, **b** initial Cr(VI) concentration, **c** pH, **d** ionic strength, **e** total hardness, and **f** sulfate, silicate, and carbonate in remediation of Cr(VI) by S-nZVI from ultrapure water. For the experiments demonstrated in **b**, **c**, **d**, **e**, and **f**, mass concentration of S-nZVI was 1 g L^{-1}. Initial Cr(VI) concentration corresponding to **a**, **c**, **d**, **e**, and **f** was 20 mg L^{-1}

mass concentration of S-nZVI until a dosage of 1 g L^{-1}, with an equilibrium pH of 7.85 (Fig. 2a). The addition of S-nZVI beyond 1 g L^{-1} caused marginal Cr(VI) reduction. Therefore, an optimum dosage of 1 g L^{-1} was chosen for all subsequent experiments. Cr(VI) removal efficiency was inversely proportional to the initial concentration of Cr(VI) (Fig. 2b). A reduction of 89% Cr(VI) was achieved for 2 mg L^{-1} initial concentration, and the removal efficiency gradually decreased to 29% in 100 mg L^{-1} Cr(VI) containing solution. Although S-nZVI addition resulted in pH increase in Fig. 2a, decrease in pH was observed due to the spiking of very high concentration of Cr(VI) as $K_2Cr_2O_7$ in Fig. 2b. The role of pH is critical in the immobilization of Cr(VI). For a similar initial Cr(VI) concentration, decrease in pH resulted in a sharp increase in Cr(VI) removal with approximately 100% of dissolved Cr(VI) remediation below pH 5 (Fig. 2c). Principle mechanisms behind Cr(VI) remediation by S-nZVI are the reduction of Cr(VI) to insoluble Cr(III) followed by coprecipitation in the form of $FeCr_2O_{4(s)}$, and adsorption of Cr(VI) on the surface of S-nZVI (Lv et al. 2019). Variation in redox-potential (E_H) with pH for a chromium water system shows the dominance of Cr(III) species at lower pH (Rai et al. 1989; Bhattacharya et al. 2020), which is indicative of the feasibility of the formation of stable Cr(III) phases in the presence of appropriate reducing materials like S-nZVI. Furthermore, the pZC value of S-nZVI was 8.36 (Section S3, Figure S1), which is comparable to the pH_{pzc} value of 8.3, previously reported by Lv et al. 2019 (Lv et al. 2019). Therefore, electrostatics facilitated the adsorption of negatively charged dissolved CrO_4^{2-} (pH > 6.51) or $HCrO_4^-$ (pH < 6.51) on the positively charged S-nZVI surface at pH below 8.3. With the decrease in pH, $HCrO_4^-$ becomes the dominant form of Cr(VI) (Bhattacharya et al. 2020). The E_H^0 values for the transformation from $HCrO_4^-$ to Cr^{3+} and CrO_4^{2-} to Cr^{3+} are 1.35 V and 0.56 V, respectively (Gustafsson 2011; Peng and Guo 2020). Since $HCrO_4^-$ is a better oxidant than CrO_4^{2-}, the reduction of Cr(VI) occurs to a higher extent at lower pH (Peng and Guo 2020). These were further supported from the removal of 76%, 83%, 87%, and 99% of Cr(VI) at the respective pH values of 8.5, 7, 6, and 5 (Fig. 2c).

Increase in the ionic strength of the background solution from 1 to 100 mM largely enhanced Cr(VI) removal from 37 to 94% (Fig. 2d). Past researchers elucidated that at higher ionic strength, passivation of precipitated iron-containing phases on S-nZVI might be prevented due to diffusion, ensuring continuous electron transfer between Fe, S, and Cr(VI) (Rangsivek and Jekel 2005; Lv et al. 2019). The presence of dissolved Ca and Mg affected the overall remediation of Cr(VI); but the variations in the initial concentrations of Ca^{2+} and Mg^{2+} did not impact Cr(VI) remediation efficiency as it varied between 56 and 60% in the hardness range of 125–1000 mg L^{-1} as $CaCO_3$ (Fig. 2e). The equilibrium pH values were less than 7.49, and the pZC of S-nZVI was 8.36. So, there was electrostatic repulsion between positively charged S-nZVI, and Ca^{2+} and Mg^{2+}. Since the major multivalent cations typically present in groundwater have only one oxidation state and adsorption on S-nZVI is

thermodynamically not feasible, their possible interventions on Cr(VI) removal might be eliminated. However, the overall decrease in Cr(VI) removal due to the presence of Ca is noticeable. Past researchers have suggested that the decrease in efficiency can be attributed to the enhanced agglomeration of the nanoparticles due to the formation of calcium complexes (Gao et al. 2018; Xu et al. 2021a). Among the major divalent anions, dissolved SO_4^{2-} did not hinder Cr(VI) removal, but increasing silicate and even a nominal amount of (20 mg L^{-1}) carbonate caused a decrease in the removal efficiency (Fig. 2f). While the presence of SO_4^{2-} might increase the number of reactive sites as well as the overall reactivity of S-nZVI to uptake Cr (Kim et al. 2014; Gao et al. 2018), a rise in equilibrium pH was inevitable due to the addition of carbonate and silicate which caused the decrease in Cr(VI) removal.

Batch equilibration studies performed in synthetic groundwater matrix at varying pH further elucidated pH dependence in the remediation of Cr(VI) by S-nZVI. Removal efficiency decreased with an increase in pH, as well as initial Cr(VI). When the initial Cr(VI) concentration was increased in the range of 2–100 mg L^{-1}, the removal efficiency gradually decreased from 99 to 51%, 98 to 50%, 90 to 49%, and 72 to 31% at pH 4, 6, 7, and 8, respectively (Fig. 3). Cr(VI) was removed to a greater extent in synthetic groundwater as compared to the ultrapure water matrix for similar initial Cr(VI) and identical pH. From the controlled experiments performed in the ultrapure water (Fig. 2), it can be suggested that the higher ionic strength of the synthetic groundwater, containing dissolved SO_4^{2-} might be responsible for better efficiency. The USEPA drinking water limit of Cr is 0.1 mg L^{-1} (USEPA 2022). Therefore, the findings from this set of batch experiments in synthetic groundwater implied that 90% Cr(VI) remediation could be achieved at pH above 6 and below 8 in subsurface environmental water

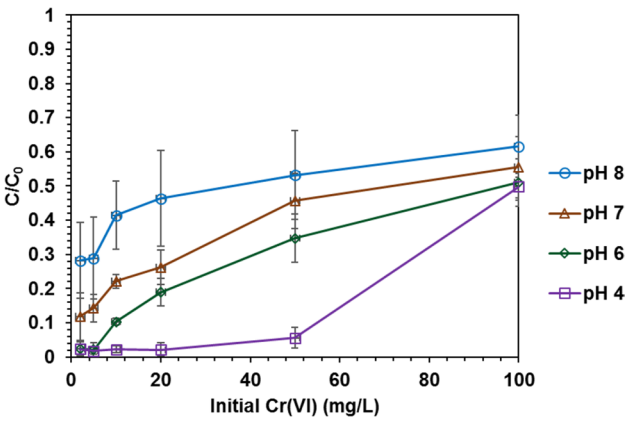

Fig. 3 Removal of varying levels of Cr(VI) from synthetic groundwater in the pH range of 4–8 by S-nZVI. All the experiments were performed in duplicates at S-nZVI dosage of 1 g L^{-1}

samples 20 times more contaminated than the permissible limit. Dissolved Cr(III) and Fe Concentrations were below the detection limit of ICP-AES (Section S5, Table S2). This observation is consistent with the results reported in one of the past studies where no dissolved Fe was found after 2 h during the reaction between Cr(VI) and S-nZVI (Lv et al. 2019).

Solid phase characterization after batch equilibration experiments was done to trace the evidence and fate of Cr on S-nZVI particles. XRD analysis confirmed the presence of iron chromite [$Cr_2FeO_{4(s)}$] in the reacted solid, indicative of precipitation of Cr as insoluble Cr(III) phase due to reduction (Fig. 4a). Similar to the synthesized material, the reacted batch of S-nZVI also contained the most intense peak of Fe^0 at 2θ 44.67. However, the FeS_2 peak diminished completely after the reaction. This result indicated that initially, FeS_2 was utilized, and Fe^0 remained as a bulk solid phase in the reacted S-nZVI. Since Fe^0 can also remove Cr(VI), the reacted S-nZVI might be recovered and reused effectively to treat another batch of Cr(VI) contaminated water. XPS of Cr 2p spectra of the reacted solid showed the peaks of Cr(III), establishing the transformation of dissolved Cr(VI) to reduced and precipitated Cr(III) (Fig. 4b). XPS analysis of the synthesized S-nZVI did not indicate any peaks of Cr before the reaction (Section S4, Figure S2). The reduction of Cr(VI) by S-nZVI, followed by the precipitation of Cr(III) due to its poor solubility, seemed to be the governing mechanism behind the immobilization of dissolved Cr(VI). Continuous electron transfer from Fe^0, Fe^{2+}, and S^- was responsible for the conversion of Cr(VI) to Cr(III) (Lv et al. 2019; Dai et al. 2022), and precipitation of $Cr_2FeO_{4(s)}$. Surface-sensitive XPS analysis further suggested the presence of Fe^{3+} in the reacted S-nZVI (Section S6, Figure S3). However, there is not enough evidence to state whether Fe^{3+} is bound to Cr(III) as $Cr_xFe_{(1-x)}(OH)_{3(s)}$, or it is simply an oxidized form of iron oxide (Fe_2O_3), resulting from partial oxidation of Fe^0. Both Fe^0 and Fe^{2+} were also traced along with Fe^{3+} on the surface of the reacted S-nZVI from XPS analysis. The spherical particles of S-nZVI (Fig. 1b) were deposited with layers of foreign particles, indicating a transformation in the morphology of the native particles due to reaction with Cr-contaminated water (Fig. 4c). Traces of Fe, S, and Cr were identified in the reacted S-nZVI particles by TEM-associated EDX area mapping (Figs. 4d–g). As suggested from the area mapping, Cr was also found to be distributed throughout the core particles of the reacted S-nZVI (Fig. 4 d and g) like Fe and S (Fig. 4e, f).

Kinetics of Cr(VI) removal from synthetic groundwater

The rate of Cr(VI) removal by S-nZVI from synthetic groundwater was quantified. The kinetic data were fitted to

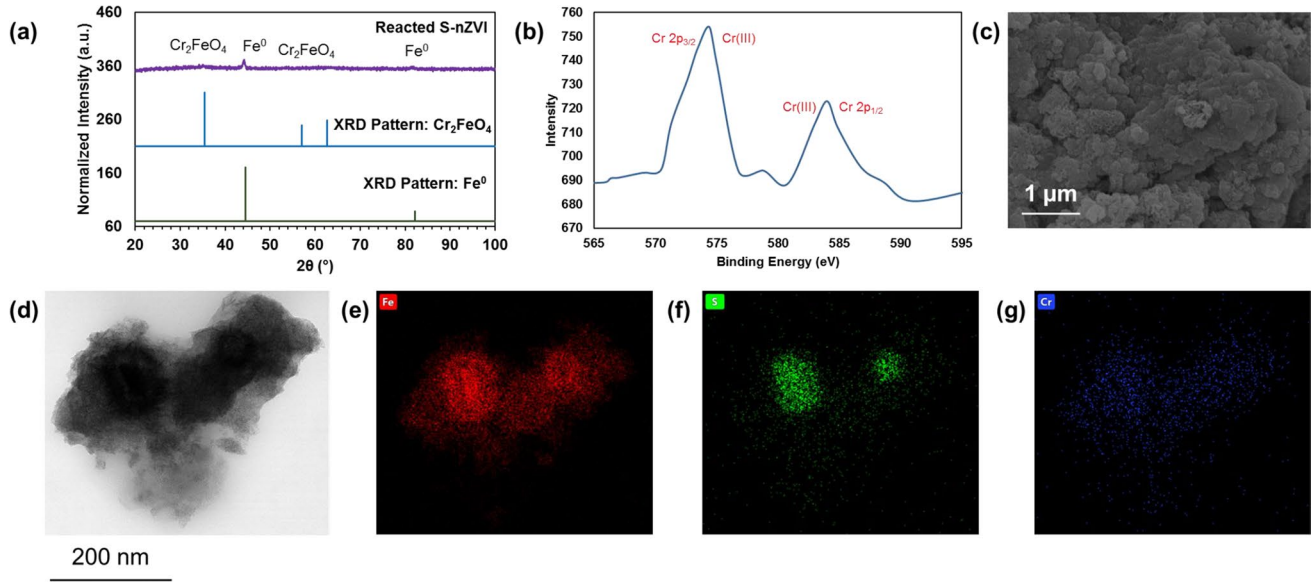

Fig. 4 **a** XRD analysis, **b** XPS analysis for Cr, **c** SEM imaging, **d** TEM imaging, and associated EDX area mapping for **e** Fe, **f** S, and **g** Cr of the solid residues recovered after batch experiments with synthetic groundwater. Identified peaks of the XRD pattern of the solid have been labeled as Cr_2FeO_4 for PDF 00–034-0140, and $Fe.^0$ for PDF 98–000-0259

the first-order and second-order reaction models. The best fit obtained by the minimum mean square error method indicated that the process of Cr(VI) immobilization by S-nZVI closely followed second-order kinetics. The respective correlation coefficient (R^2) between the experimental and modeled data of the first-order and second-order kinetics were 0.66 and 0.97 (Fig. 5). Previous studies have illustrated that the solid–liquid interfacial processes between S-nZVI and dissolved Cr(VI) at different pH in ultrapure water as well as mixed metal matrices were of pseudo second order (Gong et al. 2017; Gao et al. 2018; Chen et al. 2022; Dai et al. 2022). Modeled results of the kinetic experiment performed in the present study in a synthetic groundwater matrix were also consistent with these previous observations. The rate constant quantified from the model was 0.0035 L mg^{-1} min^{-1}. Although equilibrium was attained in 2 h, the experiment was performed for 6 h to check for any notable shifts. Measured pH values at equilibrium were 8.5 ± 0.03.

Sequential batch experiments

A comparative study was performed to estimate the extent of Cr(VI) removal due to repetitive usage of nZVI and S-nZVI. While nZVI was able to remove 88% of Cr(VI) from the first batch of Cr(VI)-spiked ultrapure water, remediation of 76% Cr(VI) was observed by S-nZVI (Fig. 6a). Robust electron transfer from Fe^0 was responsible for higher Cr(VI) reduction in the case of pure nZVI as compared to S-nZVI. However, due to the continuous usage of the recovered solid particles in the subsequent batches of water, the efficiency of nZVI gradually went down to 68% in the fourth cycle. In contrast, the performance of S-nZVI progressively improved to an efficiency of 91% in the fourth batch (Fig. 6a). A decline in

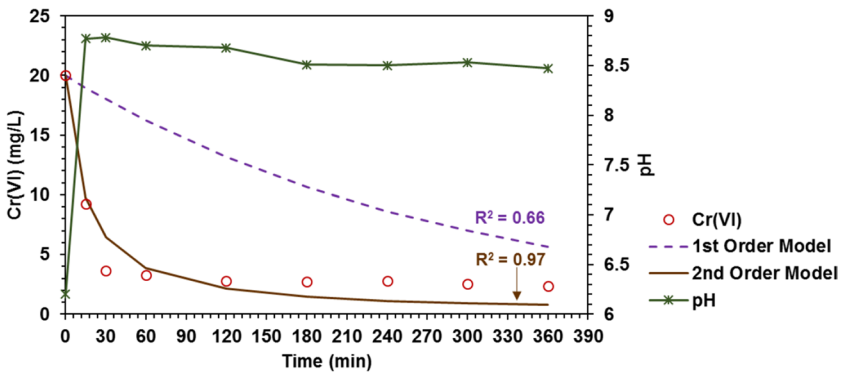

Fig. 5 Kinetic modeling of Cr(VI) remediation by S-nZVI from synthetic groundwater. All the reactors containing 20 mg L^{-1} Cr(VI) were dosed with 1 g L^{-1} S-nZVI

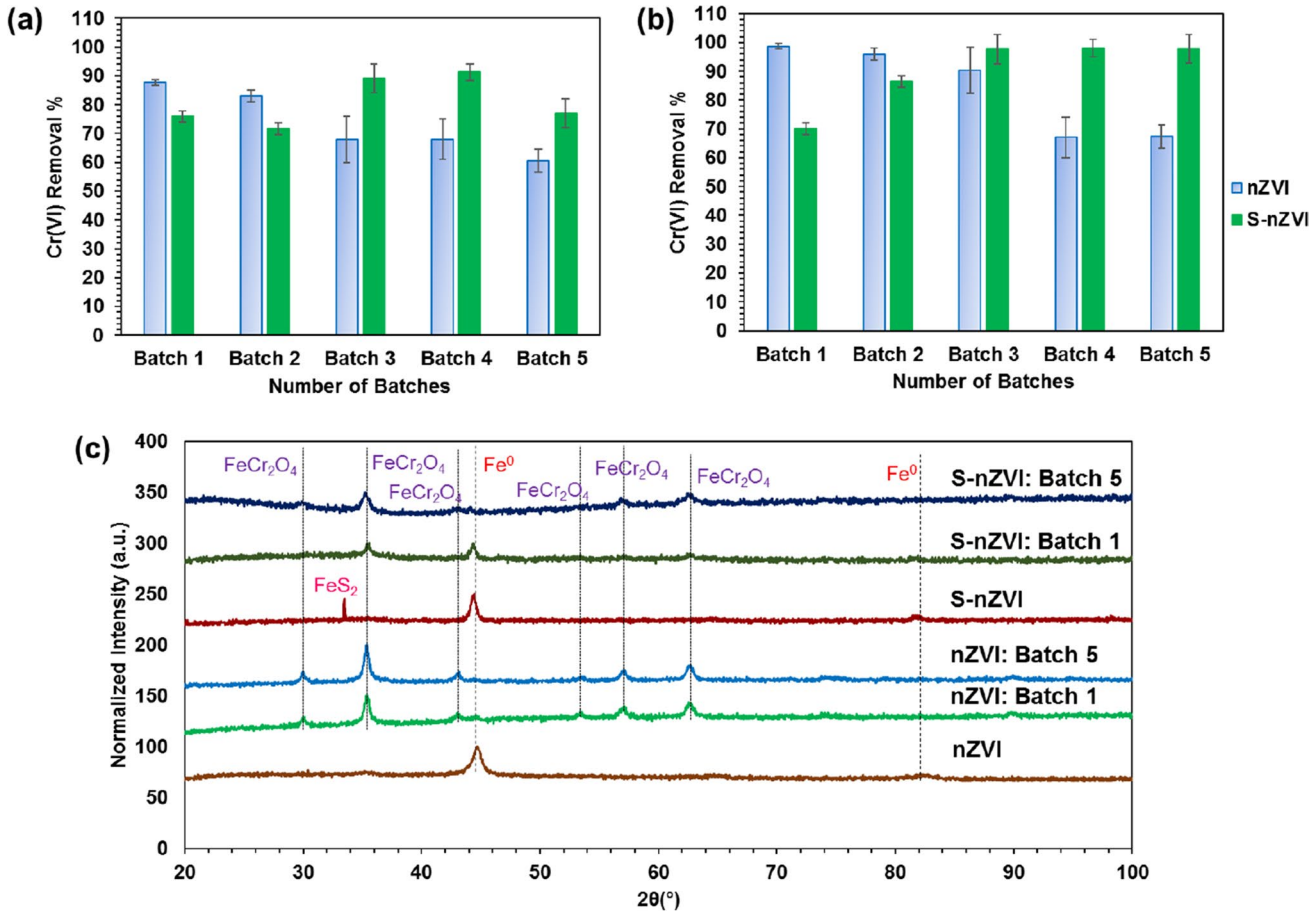

Fig. 6 Comparative removal of Cr(VI) by nZVI and S-nZVI in sequential batch reactors in **a** ultrapure water and **b** synthetic groundwater matrices; **c** XRD analysis of nZVI and S-nZVI, and the solid residues recovered after first and fifth batches during the sequential reaction experiment. Identified peaks of the XRD pattern of the solid have been labeled as $FeCr_2O_4$ for PDF 98–000-0161, $Fe.^0$ for PDF 98–000-0259, and FeS_2 for PDF 01–074-1051

the effectiveness of nZVI and S-nZVI was noted in the fifth batch with 60% and 77% respective reductions of Cr(VI). Similar to the batch experiments elaborated earlier, higher Cr(VI) reduction was achieved in the synthetic groundwater matrix as compared to the ultrapure water matrix, probably because of its higher ionic strength. The drop in removal efficiency observed in ultrapure water was not seen in the case of synthetic groundwater for five cycles. S-nZVI driven removal of Cr(VI) increased from 70 to 98% in synthetic groundwater's first and fifth cycles, respectively (Fig. 6b). However, 99% and 67% Cr(VI) removal was noticed in the first and fifth batches of nZVI-dosed synthetic groundwater, which indicated its downdrift performance (Fig. 6b).

The reason for the better performance of S-nZVI due to its prolonged and repetitive usage can be explained from the metadata: (i) Past studies demonstrated that S-nZVI caused Cr(VI) reduction due to continuous electron transfer from the iron and sulfur components present in both solid and liquid phase (Nahuel Montesinos et al. 2014; Lyu et al. 2017; Lv et al. 2019). While S-nZVI created a reducing environment; facilitated continuous electron transfer from Fe^0, Fe^{2+}, and S^-; and supported lesser exhaustion of Fe^0 due to the addition of sulfur component, rapid oxidation of Fe^0 in nZVI resulted in surface passivation. As a result, the performance of nZVI declined during the series of multiple equilibrium processes over time in spite of its high efficiency in the initial batches. (ii) Previous researchers observed that aging resulted in a drop in nZVI reactivity, possibly due to higher magnetic properties resulting in agglomeration and passivation (Guan et al. 2015). Sulfur incorporation inhibited magnetic attraction, passivation, and aggregation and aided in long-term utility (Li et al. 2016; Lv et al. 2019). (iii) Partial oxidation of S-nZVI during prolonged usage was proven to enhance Cr(VI) uptake by overcoming the rate-limiting step of surface adsorption (Liu et al. 2022).

XRD analysis performed on the solid particles collected from the first batch of reactors indicated that the Fe^0 peak almost diminished in the reacted nZVI, unlike the case of

reacted S-nZVI, where a prominent peak of Fe at 2θ 44.67° was detected (Fig. 6c). The absence of the distinguishable Fe^0 peak in the first batch of nZVI suggested rapid oxidation of iron. Although this rapid oxidation resulted in higher removal of Cr(VI) in the first batch, surface passivation of nZVI prevented its efficacy in the subsequent cycles of batches. On the other hand, $FeS_{2(s)}$ played a vital role in ensuring the extended reactive life of S-nZVI by participating in Cr(VI) immobilization. Dissolution of $FeS_{2(s)}$ can cause coprecipitation of Cr(VI) as both Fe^{2+} and reduced species of sulfur can convert Cr(VI) to insoluble Cr(III) (Patterson et al. 1997; Kim et al. 2001; Nahuel Montesinos et al. 2014; Li et al. 2017; Lyu et al. 2017). Moreover, even after the complete dissolution of the $FeS_{2(s)}$ phase, Fe^0 was identified as a prominent and trace phase in the first and fifth batches of reacted S-nZVI, respectively. As sulfur modification prevented exhaustion of Fe^0, enhanced and effective usage of S-nZVI in the treatment of multiple batches of Cr(VI)-contaminated groundwater was feasible. Precipitated $FeCr_2O_{4(s)}$ phase was identified in nZVI and S-nZVI from both the first and fifth batches, confirming the uptake of dissolved Cr(VI) in the form of reduced and insoluble Cr(III) (Fig. 6c). During the batch equilibration study, a similar form of Cr in the precipitated solid was also identified earlier in the reacted S-nZVI (Fig. 4a). More importantly, prominent Fe^0 peaks in the reacted S-nZVI have been confirmed in the batch equilibration studies as well as the sequential batch experiment (Figs. 4a and 6c). The Cr(VI) removal mechanism by S-nZVI involved the adsorption of diffused Cr(VI), reduction associated coprecipitation by iron and sulfur components present in the solid, and reduction by dissolved Fe^{2+} and dissolved reduced form of sulfur present in the liquid. A below-detectable level of soluble Cr(III) and dissolved total-Fe in batch studies further supported this hypothesis and satisfied the fundamental mechanisms of Cr(VI) removal by S-nZVI proposed in the recent studies (Lv et al. 2019; Dai et al. 2022).

In recent times, several researchers probed and reported different aspects of the benefits of S-nZVI in Cr(VI) remediation. These advantages include the preservation of the inner core of Fe^0 below a layer of FeS (Gao et al. 2018), and the prevention of aggregation of particles that results in a high specific surface area for Cr(VI) adsorption followed by its reduction (Gong et al. 2017). Moreover, Fe dissolution is retarded, aiding neutralizing the secondary contamination of Fe (Gong et al. 2017; Lv et al. 2019). Partial oxidation of nano-FeS enhances Cr(VI) removal because of increased binding affinity (Liu et al. 2022). In-situ addition of S-nZVI decreases Cr(VI) concentration and maintains a long-term low redox potential in groundwater, favoring stable precipitation of insoluble Cr(III) and co-existence of Fe^0 in high quantity even after several months of injection (Brumovský et al. 2021). All these findings are consistent with the results of the present study, where we observed utilization of FeS_2 and lesser usage of Fe^0 in the earlier cycles of batches aided in enhanced Cr(VI) removal during repetitive usage of S-nZVI in Cr(VI)-contaminated water matrices.

Conclusions

S-nZVI was synthesized and characterized in the laboratory to remove dissolved Cr(VI) in multiple cycles of batches. XRD analysis indicated the presence of Fe^0 and FeS_2, and TEM-associated EDX mapping confirmed the existence of both iron and sulfur in the synthesized S-nZVI. Batch experiments in the ultrapure water matrix elucidated that Cr(VI) removal increased with the rise in ionic strength and decreased with high initial Cr(VI), pH, carbonate, and silicate. The presence of sulfate in the range of 20–200 mg L^{-1} facilitated very high (97–99%) remediation of Cr(VI), unlike other cations or anions. For similar pH and initial Cr(VI), S-nZVI showed better performance in synthetic groundwater matrix, indicating the suitability of the material in treating aquifers containing 2 mg L^{-1} Cr(VI), which is 20 times more than its permissible limit. Moreover, the sequential batch extraction experiments were meant to establish the cost-effective application of S-nZVI in groundwater treatment. In addition, the experiments were performed with an initial Cr(VI) of 20 mg L^{-1}, which is 200 times more than the permissible limit. Repetitive elevated effectiveness of S-nZVI through the removal of more than 97% Cr(VI), even in such highly contaminated groundwater, suggests its suitability over conventional nZVI. Coating of $FeS_{2(s)}$ favored prolonged reducing environment, inhibited exhaustion of Fe^0, and supported adsorption of diffused Cr(VI), reduction of Cr(VI) due to direct electron transfer from reduced forms of iron and sulfur in both solid and liquid phase, and coprecipitation. However, rapid oxidation of Fe^0 created surface passivation of nZVI, ensuing performance declination during repeated application. The Cr(VI) removal rate from synthetic groundwater was quantified as 0.0035 L mg^{-1} min^{-1}. The kinetic data fitted with the second-order reaction rate model with R^2 0.97. Overall, the results indicated that with 1 g L^{-1} S-nZVI, a minimum of five batches of 20 mg L^{-1} Cr(VI) contaminated groundwater can be treated with 98% efficiency, implying a potential benefit for its application over conventional nZVI. Increasing removal of Cr(VI) even after multiple time usage of S-nZVI indicated its efficient long-term performance. Therefore, the associated treatment cost might be lower than that of the nZVI-based purification technique. This study will facilitate the application of S-nZVI for Cr(VI) removal from groundwater and could provide a pathway to treat other groundwater contaminants.

Supplementary Information The online version contains supplementary material available at https://doi.org/10.1007/s11356-023-30960-4.

Acknowledgements Laboratory facilities provided to Prof. Swatantra Pratap Singh in the Environmental Science and Engineering Department of Indian Institute of Technology Bombay are duly acknowledged. Central facilities supported by the Industrial Research Consultancy Centre in Indian Institute of Technology Bombay for XRD and TEM analysis in Metallurgical Engineering and Material Science, Central Surface Analytical Facility in Physics department for XPS analysis, and SEM-EDX analysis in FEG-SEM laboratory in Sophisticated Analytical Instrument Facility of Indian Institute of Technology Bombay are also sincerely acknowledged.

Author contribution All authors contributed to the study conception and design. Material preparation and characterization were done by Mainak Bhattacharya and Najmul Haque Barbhuiya. Data collection and analysis were performed by Mainak Bhattacharya. Ideas for the experimentation were shared by Swatantra Pratap Singh. The first draft of the manuscript was written by Mainak Bhattacharya, and all authors commented on previous versions of the manuscript. All authors read and approved the final manuscript.

Funding The authors received financial assistance from the Department of Science and Technology (DST)-Scheme for Young Scientists and Technologists (SYST, SP/YO/2019/1579), Government of India, for the project; Institute Post Doctoral Fellowship of Indian Institute of Technology Bombay provided to Dr. Mainak Bhattacharya; and Prime Minister Research Fellowship provided by the Government of India to Ph.D. student Najmul Haque Barbhuiya. Prof. Swatantra Pratap Singh also received research fund provided by the Department of Science and Technology, Government of India under DST-Inspire scheme.

Declarations

Ethics approval Not applicable.

Consent to participate Not applicable.

Consent to publication All the authors of this manuscript give full consent to publish this research. No further consent is required from any organizations or individual.

Competing interests The authors declare no competing interests.

References

Bacquart T, Frisbie S, Mitchell E et al (2015) Multiple inorganic toxic substances contaminating the groundwater of Myingyan Township, Myanmar: arsenic, manganese, fluoride, iron, and uranium. Sci Total Environ 517:232–245. https://doi.org/10.1016/j.scitotenv.2015.02.038

Bhattacharya M, Shriwastav A, Bhole S et al (2020) Processes governing chromium contamination of groundwater and soil from a chromium waste source. ACS Earth Sp Chem 4:35–49. https://doi.org/10.1021/acsearthspacechem.9b00223

Brumovský M, Oborná J, Lacina P et al (2021) Sulfidated nano-scale zerovalent iron is able to effectively reduce in situ hexavalent chromium in a contaminated aquifer. J Hazard Mater 405. https://doi.org/10.1016/j.jhazmat.2020.124665

Cao Z, Li H, Lowry GV et al (2021) Unveiling the role of sulfur in rapid defluorination of florfenicol by sulfidized nanoscale zero-valent iron in water under ambient conditions. Environ Sci Technol 55:2628–2638. https://doi.org/10.1021/acs.est.0c07319

Chen M, Xu H, Zhang Y et al (2022) Effective removal of heavy metal ions by attapulgite supported sulfidized nanoscale zerovalent iron from aqueous solution. Colloids Surfaces A Physicochem Eng Asp 640:128192. https://doi.org/10.1016/j.colsurfa.2021.128192

Dai Y, Duan L, Du W et al (2022) Morphology and structure of in situ FeS affect Cr(VI) removal by sulfidated microscale zero-valent iron with short-term ultrasonication. Chemosphere 290. https://doi.org/10.1016/j.chemosphere.2021.133372

Deng M, Wang X, Li Y et al (2020) Reduction and immobilization of Cr(VI) in aqueous solutions by blast furnace slag supported sulfidized nanoscale zerovalent iron. Sci Total Environ 743:140722. https://doi.org/10.1016/j.scitotenv.2020.140722

Fan D, Lan Y, Tratnyek PG et al (2017) Sulfidation of iron-based materials: a review of processes and implications for water treatment and remediation. Environ Sci Technol 51:13070–13085. https://doi.org/10.1021/acs.est.7b04177

Gao J, Yang L, Liu Y et al (2018) Scavenging of Cr(VI) from aqueous solutions by sulfide-modified nanoscale zero-valent iron supported by biochar. J Taiwan Inst Chem Eng 91:449–456. https://doi.org/10.1016/j.jtice.2018.06.033

Gheju M (2011) Hexavalent chromium reduction with zero-valent iron (ZVI) in aquatic systems. Water Air Soil Pollut 222:103–148. https://doi.org/10.1007/s11270-011-0812-y

Gong Y, Gai L, Tang J et al (2017) Reduction of Cr(VI) in simulated groundwater by FeS-coated iron magnetic nanoparticles. Sci Total Environ 595:743–751. https://doi.org/10.1016/j.scitotenv.2017.03.282

Gu Y, Gong L, Qi J et al (2019) Sulfidation mitigates the passivation of zero valent iron at alkaline pHs: experimental evidences and mechanism. Water Res 159:233–241. https://doi.org/10.1016/j.watres.2019.04.061

Guan X, Sun Y, Qin H et al (2015) The limitations of applying zero-valent iron technology in contaminants sequestration and the corresponding countermeasures: the development in zero-valent iron technology in the last two decades (1994–2014). Water Res 75:224–248. https://doi.org/10.1016/j.watres.2015.02.034

Gustafsson JP (2011) Visual MINTEQ

Hu H, Zhao D, Wu C, Xie R (2022) Sulfidized nanoscale zerovalent iron supported by oyster powder for efficient removal of Cr (VI): Characterization, performance, and mechanisms. Materials (basel) 15:3898

ICDD (2013) Powder Diffraction File

International Centre for Diffraction Data (2010) MDI JADE

Kanagaraj G, Elango L (2019) Chromium and fluoride contamination in groundwater around leather tanning industries in southern India: Implications from stable isotopic ratio Δ53Cr/Δ52Cr, geochemical and geostatistical modelling. Chemosphere 220:943–953. https://doi.org/10.1016/j.chemosphere.2018.12.105

Kim C, Zhou Q, Deng B et al (2001) Chromium(VI) reduction by hydrogen sulfide in aqueous media: stoichiometry and kinetics. Environ Sci Technol 35:2219–2225. https://doi.org/10.1021/es0017007

Kim HS, Ahn JY, Kim C et al (2014) Effect of anions and humic acid on the performance of nanoscale zero-valent iron particles coated with polyacrylic acid. Chemosphere 113:93–100. https://doi.org/10.1016/j.chemosphere.2014.04.047

Li D, Mao Z, Zhong Y et al (2016) Reductive transformation of tetrabromobisphenol A by sulfidated nano zerovalent iron. Water Res 103:1–9. https://doi.org/10.1016/j.watres.2016.07.003

Li Y, Wang W, Zhou L et al (2017) Remediation of hexavalent chromium spiked soil by using synthesized iron sulfide particles. Chemosphere 169:131–138. https://doi.org/10.1016/j.chemosphere.2016.11.060

Liu Y, Gan H, Tian L et al (2022) Partial oxidation of FeS nanoparticles enhances Cr(VI) sequestration. Environ Sci Technol 56:13954–13963. https://doi.org/10.1021/acs.est.2c02406

Lv D, Zhou J, Cao Z et al (2019) Mechanism and influence factors of chromium(VI) removal by sulfide-modified nanoscale zerovalent iron. Chemosphere 224:306–315. https://doi.org/10.1016/j.chemosphere.2019.02.109

Lyu H, Tang J, Huang Y et al (2017) Removal of hexavalent chromium from aqueous solutions by a novel biochar supported nanoscale iron sulfide composite. Chem Eng J 322:516–524. https://doi.org/10.1016/j.cej.2017.04.058

Mahmood T, Saddique MT, Naeem A et al (2011) Comparison of different methods for the point of zero charge determination of NiO. Ind Eng Chem Res 50:10017–10023. https://doi.org/10.1021/ie200271d

Matern K, Weigand H, Singh A, Mansfeldt T (2017) Environmental status of groundwater affected by chromite ore processing residue (COPR) dumpsites during pre-monsoon and monsoon seasons. Environ Sci Pollut Res 24:3582–3592. https://doi.org/10.1007/s11356-016-8110-2

Nahuel Montesinos V, Quici N, Beatriz Halac E et al (2014) Highly efficient removal of Cr(VI) from water with nanoparticulated zerovalent iron: understanding the Fe(III)-Cr(III) passive outer layer structure. Chem Eng J 244:569–575. https://doi.org/10.1016/j.cej.2014.01.093

Patterson RR, Fendorf S, Fendorf M (1997) Reduction of hexavalent chromium by amorphous iron sulfide. Environ Sci Technol 31:2039–2044. https://doi.org/10.1021/es960836v

Peng H, Guo J (2020) Reduction behavior of chromium(VI) with oxalic acid in aqueous solution. Sci Rep 10:1–8. https://doi.org/10.1038/s41598-020-74928-7

Poonia T, Singh N, Garg MC (2021) Contamination of arsenic, chromium and fluoride in the Indian groundwater: a review, meta-analysis and cancer risk assessment. Int J Environ Sci Technol 18:2891–2902. https://doi.org/10.1007/s13762-020-03043-x

Qin G, McGuire MJ, Blute NK et al (2005) Hexavalent chromium removal by reduction with ferrous sulfate, coagulation, and filtration: a pilot-scale study. Environ Sci Technol 39:6321–6327. https://doi.org/10.1021/es050486p

Rai D, Sass BM, Moore DA (1987) Chromium(III) hydrolysis constants and solubility of chromium(III) hydroxide. Inorg Chem 26:345–349. https://doi.org/10.1021/ic00250a002

Rai D, Eary LE, Zachara JM (1989) Environmental chemistry of chromium. Sci Total Environ 86:15–23. https://doi.org/10.1016/0048-9697(89)90189-7

Rangsivek RÃ, Jekel MR (2005) Removal of dissolved metals by zero-valent iron (ZVI): kinetics, equilibria, processes and implications for stormwater runoff treatment. Water Res 39:4153–4163. https://doi.org/10.1016/j.watres.2005.07.040

Santra D, Mandal S, Santra A, Ghorai UK (2018) Cost-effective, wireless, portable device for estimation of hexavalent chromium, fluoride, and iron in drinking water. Anal Chem 90:12815–12823. https://doi.org/10.1021/acs.analchem.8b03337

Sass BM, Rai D (1987) Solubility of amorphous chromium(III)-iron(III) hydroxide solid solutions. Inorg Chem 26:2228–2232. https://doi.org/10.1021/ic00261a013

Sharma SK, Petrusevski B, Amy G (2008) Chromium removal from water: a review. J Water Supply Res Technol - AQUA 57:541–553. https://doi.org/10.2166/aqua.2008.080

Shen W, Xu J, Zhu L (2021) Triton X-100 improves the reactivity and selectivity of sulfidized nanoscale zerovalent iron toward tetrabromobisphenol A: implications for groundwater and soil remediation. J Hazard Mater 416:126119. https://doi.org/10.1016/j.jhazmat.2021.126119

Turick CE, Apel WA, Carmiol NS (1996) Isolation of hexavalent chromium-reducing anaerobes from hexavalent-chromium-contaminated and noncontaminated environments. Appl Microbiol Biotechnol 44:683–688. https://doi.org/10.1007/BF00172503

USEPA (1992) Method 7196A: Chromium, hexavalent (colorimetric), test methods for evaluating solid waste, physical/chemical methods-SW-846. US Environment Protection Agency Washigton DC

USEPA (2022) Chromium in drinking water. https://www.epa.gov/sdwa/chromium-drinking-water. Accessed 25 Aug 2022

Wei X, Guo Z, Yin H et al (2021) Removal of heavy metal ions and polybrominated biphenyl ethers by sulfurized nanoscale zerovalent iron: compound effects and removal mechanism. J Hazard Mater 414:125555. https://doi.org/10.1016/j.jhazmat.2021.125555

Xi Y, Wu Y, Liu Y et al (2022) Covering extracellular polymeric substances to enhance the reactivity of sulfidated nanoscale zerovalent iron toward Cr(VI) removal. Chem Eng J 448:137610. https://doi.org/10.1016/j.cej.2022.137610

Xu J, Wang Y, Weng C et al (2019) Reactivity, selectivity, and long-term performance of sulfidized nanoscale zerovalent iron with different properties. Environ Sci Technol 53:5936–5945. https://doi.org/10.1021/acs.est.9b00511

Xu J, Avellan A, Li H et al (2020a) Iron and sulfur precursors affect crystalline structure, speciation, and reactivity of sulfidized nanoscale zerovalent iron. Environ Sci Technol 54:13294–13303. https://doi.org/10.1021/acs.est.0c03879

Xu J, Li H, Lowry GV (2021b) Sulfidized nanoscale zero-valent iron: tuning the properties of this complex material for efficient groundwater remediation. Accounts Mater Res 2:420–431. https://doi.org/10.1021/accountsmr.1c00037

Xu J, Avellan A, Li H et al (2020b) Sulfur loading and speciation control the hydrophobicity, electron transfer, reactivity, and selectivity of sulfidized nanoscale zerovalent iron. 32:1–10. https://doi.org/10.1002/adma.201906910

Xu H, Gao M, Hu X et al (2021a) A novel preparation of S-nZVI and its high efficient removal of Cr(VI) in aqueous solution. J Hazard Mater 416. https://doi.org/10.1016/j.jhazmat.2021.125924

Yao Y, Mi N, He C et al (2020) Humic acid modified nano-ferrous sulfide enhances the removal efficiency of Cr(VI). Sep Purif Technol 240. https://doi.org/10.1016/j.seppur.2020.116623

Yu J, Yang S, Liu D et al (2023) Interaction of chromium-sulfur-iron during Cr(VI) stabilization by polysulfide-modified nanoscale zero-valent iron for groundwater remediation: batch experiments and numerical simulation. Chem Eng J 475:146233. https://doi.org/10.1016/j.cej.2023.146233

Zhao R, Cao X, Li T et al (2022) Co-removal effect and mechanism of Cr(VI) and Cd(II) by biochar-supported sulfide-modified nanoscale zero-valent iron in a binary system. Molecules 27. https://doi.org/10.3390/molecules27154742

Zhou C, Han C, Min X, Yang T (2022) Effect of different sulfur precursors on efficient chromium(VI) removal by ZSM-5 zeolite supporting sulfide nano zero-valent iron. Chem Eng J 427:131515. https://doi.org/10.1016/j.cej.2021.131515